CrossMark

Design Optimization and Development of Tubular Isogrid Composites Tubes for Lower Limb Prosthesis

Diego Morais Junqueira[1] · Guilherme Ferreira Gomes[1] ·
Márcio Eduardo Silveira[2] · Antonio Carlos Ancelotti Jr[1]

Abstract From the beginnings of humanity, natural or unnatural misfortunes such as illnesses, wars, automobile accidents cause loss of body limbs like teeth, arms, legs, etc. The solution found for the replacement of these missing limbs is in the use of prostheses. Lower limbs tubes or pylons are prosthetics components that are claimed to support loads during walking and other daily tasks activities. Commonly, prosthetic tubes are manufactured using metal materials such as stainless steel, aluminum and titanium. The mass of these tubes is generally high compared to tubes made of carbon fiber reinforced polymer matrix (CFRP) composite. Therefore, this work has the objective of design, manufacturing and analyzing the feasibility of a new tube concept, made of composite material, which makes use of lattice structure and inner layer. Until the present moment, lower limb prosthesis tubes using lattice structure and ineer layer have never been studied and/or tested to date. It can be stated that the tube of rigid ribs with inner layer and angle of 40° is more efficient than those of 26° and 30°. The proposed design allows a structural weight reduction in high performance prostheses from 120 g to 40 g.

Keywords Pylon · Transtibial prosthesis · Lattice structure · Isogrid · Finite element method

Nomenclature
Φ Angle of helical ribs with respect to the axial axis of the structure
δ_h Width of helical ribs
δ_c Width of circular ribs
α_h Distance between helical ribs
α_c Distance between circular ribs

✉ Guilherme Ferreira Gomes
guilhermefergom@unifei.edu.br

[1] Mechanical Engineering Institute, Federal University of Itajubá (UNIFEI), Av. BPS, 1303, Itajubá 37500-903, Brazil

[2] Department of Mechanical Engineering, Federal University of São João Del-Rey (UFSJ), Frei Orlando, 170, São João Del Rei 36307-352, Brazil

ρ_h Specific mass of the augers
$\bar{h}$ Average thickness of rigid ribs
$\overline{\delta_h}$ Average width of helical ribs
$\overline{\delta_c}$ Average width of circular ribs
$\overline{\rho}$ Average specific mass of rigid ribs
σ_h Helical ribs rupture stress
σ_c Circular ribs rupture stress
D Diameter of the isogrid tube
E_c Circular ribs modulus of elasticity
E_h Modulus of elasticity of the helical ribs
h Thickness of the isogrid
k Buckling factor
L Length of the isogrid tube
M Structure mass
P Loading factor

1 Introduction

Lower limbs tubes or pylons are prosthetics components that are claimed to support loads during walking and other daily tasks activities, i.e., in lower limb amputations, when attached to a socket replaces the role of the tibia and fibula bones as support structure [1]. Usually, in the market and literature, prosthetic tubes are fabricated using metallic materials such as stainless steel, aluminum and titanium steels [2]. The mass of these tubes is generally high compared to tubes made of Carbon Fiber Reinforced Polymer.

For the manufacture of prosthetic tubes in composite materials, a number of processes may be adopted, which should be adapted to the geometric complexity, thickness, length and cost. Some processes currently used for the manufacture of prosthetic tubes are: Filament winding, pultrusion, use of pre-impregnated with bladder molding and vacuum assisted resin infusion molding (VARTM).

The prosthetic tube studied in the present study is characterized by its high mechanical resistance associated with its low weight. Even in comparison with the follow-up of tubes in composite materials with carbon fiber reinforcement, their weight is much smaller and their mechanical properties have fair values. Its difference from traditional prosthetic tubes is to have rigid helical and hoop ribs serving as structural reinforcement. The intersection between the helical and hoop ribs, which are known as knots, form triangles that guarantee stability, stiffness and mass relief for the structure. In addition, the prosthetic tube has an inner layer of structural support made of polymer.

As an alternative to the lower limb prosthesis tubes available in the market and literature, the main objective of this work is to design, manufacture and analyze the feasibility of a new concept of a prosthetic tube, made of composite material, which makes use of a grid stiffened structure and polymeric inner layer. This new concept of a prosthetic tube will generate a greater savings of material in view that it will be necessary a smaller amount of carbon fiber to carry out its manufacture. The design of the prosthetic tube using grid stiffened structure was performed by finite element method and the experimental validation was carried out with the manufacturing of a carbon fiber composite isogrid tube. It can be

stated that the tube of rigid ribs with inner layer and angle of 40° is more efficient than those of 26° and 30°.

Most of the lower limb prosthesis tubes are manufactured from metallic materials, which leads to heavier tubes. From the user's point of view, a lighter, sturdy tube directly implies a greater comfort and greater safety to walk and perform daily tasks. Although composite material technology is widespread in both academia and industry, prosthetic tubes for lower limb amputations using lattice structures have never been studied and/or tested. To the authors' best knowledge, there are no (or very scarce) studies in the literature about the influence of inserting an inner layer on lattice structures as well as its effects on the mechanical properties of the tube, especially for transtibial prosthesis. It is a study from the point of view of the use of a new concept of structure applied to tubes for prostheses of lower limbs with potential to be alternative to the tubes present in the market and literature.

The main contribution of the research developed is the development of isogrid structure in carbon fiber prosthetic tubes. The novelty of the developed structure allows a structural weight reduction in high performance prostheses from 120 g (conventional) to 40 g (this work).

The remaining manuscript is organized as follows: Section 2 presents a review of the literature. Section 3 presents information on the materials used, and the methodology for the design, fabrication and validation of prosthetic tubes by numerical analysis and mechanical tests. Section 4 shows the results obtained by numerical and experimental simulation. Finally, Section 5 presents the overall conclusion of this paper.

2 Backgrounds

2.1 Biomechanical Prosthesis

From the beginnings of humanity, natural or unnatural misfortunes such as illnesses, wars, automobile accidents, etc., cause loss of body limbs like teeth, arms, legs, etc. [3]. The solution found for the replacement of these missing limbs is in the use of prostheses. The term "*prosthesis*" originates from the Greek verb "*prostithenai*" whose meaning is "*put in place*".

The earliest prostheses that have registration had their origin in ancient Egypt. Because of their rudimentary configurations, these prostheses were used as a complement to the body rather than being functional. However, recently scientists have reported finding the first prosthetic finger made from a functional wood in an ancient mummy in Egypt [4].

Over time, the design of the prostheses has been improving in relation to its functional aspect. In 1858, in the city of Capua, Italy, an artificial leg dating from 300 BC, made of bronze and iron with a wooden nucleus, apparently with functional use in lower limb amputation [4], was unearthed. In 1560, the French surgeon Ambroise Paré and the French artisan Le Petit Lorrain designed a functional and revolutionary prosthetic leg made of metal, leather, paper and glue. The prosthesis for amputation of the lower limb makes use of a mechanism of activation by cord ensuring certain mobility to the user [5].

During the seventeenth century until the mid-nineteenth century, several concepts of prostheses were developed as in the case of Pieter Verduyn who, in 1696, designed the first prosthesis with mobile joints becoming a reference for future prostheses with joints that allow degrees of freedom to the user. As early as 1800, a Londoner named James Potts developed a

prosthesis for lower limb amputation made of wood which became known as "*Anglesey Leg*". In 1839, William Selpho took the Prosthesis of Potts to the United States and developed the prosthesis that would be called "*Selpho Leg*". The development of prostheses continued to grow in the nineteenth century until arriving in 1912 when aviator Marcel Desoutter, who lost his leg in World War I, designed and manufactured the first aluminum prosthesis in history [4].

According to [6], after the invention of the SACH prosthetic foot in the late 1950s, the design and types of materials used in the manufacture of prostheses did not change much. However, in the 1980s, a flexible prosthetic foot was fabricated using two carbon fiber laminates, lightweight, sturdy and high strength mechanical material that until then had been used predominantly in the aeronautics industry.

The first model of transtibial prosthesis made entirely of composite material was developed by Van L. Phillips in 1983 [7]. This model proposed by Phillips encompasses the joining of a prosthetic foot with extension to the stump.

From Ambroise Paré and Le Petit Lorrain, in 1560, began the introduction of new non-conventional materials, conceptually called low resistance composite materials, for the manufacture of prostheses. However, using the Van L. Phillips prosthesis, the use of high-strength composite materials for the manufacture of high-performance and user-friendly prostheses was initiated.

With the advancement in the development of new composite materials, mainly with the use of carbon fiber and thermosetting resins, it was possible a great advance in the design of new prostheses and orthopedic appliances [8]. At the 1988 Olympics, a flexible prosthetic foot was used for the first time in a sports race. In 1992, several models of running prostheses made of composite material were developed as the case of the Cheetah (Össur), flex-sprint (Össur), flex-run (Össur), sprinter (Otto Bock) and C-sprint Otto Bock) illustrated in Fig. 1 [6].
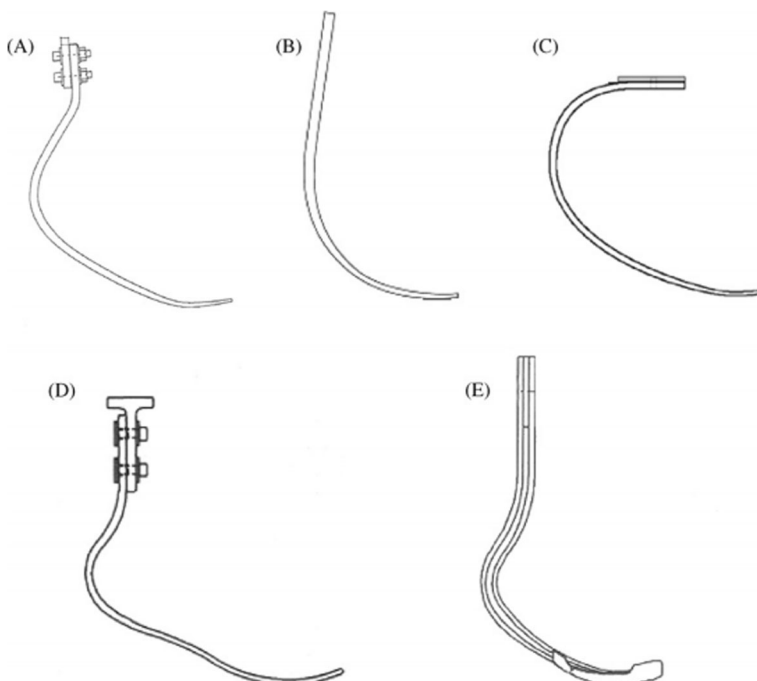
Fig. 1 Prosthesis of running: (**a**) Cheetah, (**b**) flex-sprint, (**c**) flex-run, (**d**) sprinter and (**e**) C-sprint [6]

Thus, the development of transtibial prostheses has undergone a constant evolution of design and selection of materials from the twentieth century to the most sophisticated prostheses in polymer composites today.

According to [7], transtibial amputation or lower limb amputation can be defined as that performed between the knee joint and tibiotarsal disarticulation, and can be divided into three levels: proximal, middle and distal third.

In the case of lower-limb amputations, the use of prosthetic devices to provide the conditions for the normal functioning of the limbs, i.e., to return to walking and perform daily tasks [9]. Modular prostheses are generally composed of some structural and interchangeable components, illustrated in Fig. 2, such as the prosthetic foot, the prosthetic tube and the prosthetic tube support.

Some studies [10–12] investigated the biomechanical effects of transtibial prostheses and their relationship with locomotion (walking) of people with lower limb amputations. These studies have demonstrated the efficiency of transtibial prostheses in providing the necessary bodily support for the users in addition to restoring lost locomotor functions and altered anthropometry.

Fig. 2 Modular prosthesis for lower limb amputations: (**a**) Prosthetic tube, (**b**) Support and (**c**) Prosthetic foot
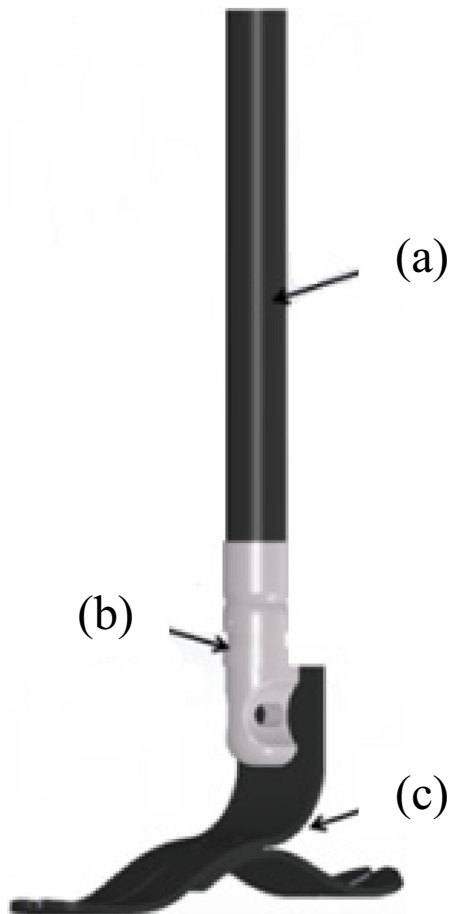
According to [13] a large number of studies investigated the effects of the design of transtibial prostheses related to biomechanical and physiological consequences on the performance of the amputee, but without considering its mechanical properties.

2.2 Prosthetic Tubes

The prosthetic tube of the English Pylon [14] is generally a structure with no welded joints or moving parts. Prosthetic tubes are usually present in modular (endoskeletal) transtibial prostheses, whereas in conventional (exoskeletal) prostheses they are incorporated into a single component formed by the junction of the foot, tube and knee. In amputations of lower limbs, when connected to a socket/ft assembly, it replaces the role of the tibia and fibula bones as support structure and load transfer during walking or running [15].

Transtibial prosthesis tubes are generally fabricated using metallic materials such as stainless steel, aluminum and titanium steels [2]. The use of thermoplastic materials in the manufacture of prosthetic tubes has been studied by several authors [16–18].

The prosthetic tube proposed by [16], was manufactured in polypropylene phomopolymer (PP) in a vacuum thermoforming process. The results obtained through fatigue tests showed that the prosthetic tube proposed by [16] supported 500,000 loading cycles without failure, that is, the tube would have a useful life corresponding to one year for a transtibial amputee walking about 1300 steps per day.

In order to reduce the cost of manufacturing transtibial prostheses, [9] studied the application of Bamboo in the manufacture of a lower limb prosthesis as an alternative to the use of "*conventional*" materials. In the case of compression tests, the prosthetic tube made of bamboo presented values of 88 MPa for compression stress and modulus of elasticity of 44 GPa. With these values, [9] compared the compression stresses of an aluminum in the annealed state (48 MPa) and fiber reinforced plastic module (12 GPa) found that bamboo is twice as tough as aluminum and three times as much as fiber reinforced plastic (FRP). In addition, he concluded that Bamboo is an excellent material with potential to be used in tubes of transtibial prostheses due to its low cost of manufacture and good structural rigidity.

Nowadays, tubes made from structural composite materials have grown strongly due to their high mechanical rigidity associated with low weight and long life in fatigue [19]. Thus, tubes for prosthetic applications made from composite materials have been studied by several authors [20–22], mainly the tubes manufactured in fiber reinforced polymer matrices (CFRP) that have brought significant gains in terms of mechanical performance and structural efficiency.

In order to obtain a cheaper prosthetic tube with good mechanical properties, [21] fabricated and tested composite tubes for transtibial prostheses using the bladder molding process (BMP) using unidirectional pre-impregnated carbon/epoxy fibers. Using numerical simulation by the finite element method, he improved the stacking sequence of the pre-impregnated material and fabricated the tubes by the BMP process. Regarding the mechanical properties obtained from the certification tests referenced by the norm NBR ISO 10328, it was verified that the pipes reached all the technical requirements of the standard, being feasible its manufacture and commercialization. In relation to the cost of the manufacturing process of the prosthetic tubes manufactured by BMP, compared to other processes such as VARTM and filament winding, it is concluded that it becomes more expensive in relation to VARTM and of the same value compared to those produced by filament winding. The main contribution of the research developed is the development of isogrid structure in carbon fiber prosthetic tubes. The novelty

of the developed structure allows a structural weight reduction in high performance prostheses from 120 g (conventional) to 40 g (this work). All this work has a total focus on industrial application in the high performance prosthesis sports industry.

In the present study, the effects of the design, stiffness and energy storage on the prosthetic foot-ankle joint were investigated [23, 24] and its influence on amputees below the knee. Some studies [25–27] analyzed the effects of alignment on the socket/support of the prosthetic tube and its reaction forces on transtibial prostheses. However, a small number of articles investigated the effects of prosthetic tube material [9, 16, 28, 29] and mechanical properties of impact absorption [30] in transtibial prostheses. In addition, a smaller number of studies considered design aspects, tensions involved, stiffness and lightness [9, 20–22]. Thus, the work developed in this research encompasses parameters not explored in the literature such as design, tensions involved, stiffness and lightness.

2.3 Isogrid Structures

Nowadays, the search for materials and structures of high performance, that is, structures that conciliate low weight and high mechanical resistance has become more common. Industry sectors with advanced engineering technology, such as the aerospace industry, have a growing demand for very light and strong parts and components capable of withstanding very high loads. The main reasons for this demand are related to the reduction of fuel consumption (with consequent reduction in the emission of pollutants) and better structural and mechanical performance of the aircraft, generating greater safety and comfort for the users, besides greater economy for the companies [31] Another sector with high growth in the search for composite materials and lighter and more resistant structures is that of biomechanics.

Isogrid or Anisogrid structures [32], have the cylindrical or conical shape. Traditionally in literature there are two types of configurations of rigid strut structures being the open and the closed. The closed structure is formed externally by a few layers of carbon fiber/epoxy or other type of composite material. Internally the structure consists of circular and helical rigid ribs made of the same material as the outer layer or other type of composite material. The circular and helical ribs intersect at points called nodes [33]. Among the nodes can form triangular or hexagonal structures whose objective and provide structural stability [32, 34]. Figure 3 shows the composition of a closed structure of rigid ribs made of carbon fiber and epoxy resin.

The open isogrid consists only of circular and helical struts without the use of the outer layer. Object of study of this work, a different configuration of structure of rigid ribs was proposed. This structure, which will be discussed in detail in Section 3, consists of an inner layer of polymer with stabilizing and structural reinforcement function.

Isogrid lattice   +   Skin   =   Assembly (Isogrid + Skin)
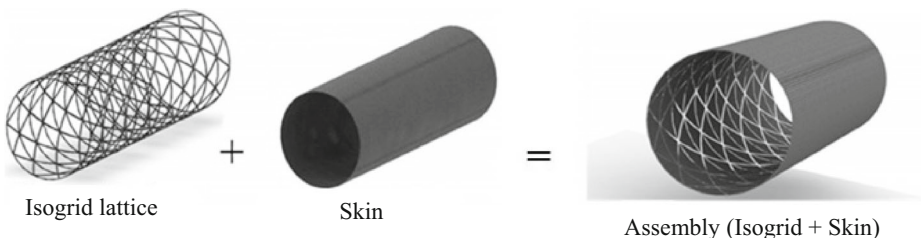
Fig. 3 Isogrid structures concept (adapted from [41])

According to [35], the term "*isogrid*" is commonly used to refer to any lattice structure whose reinforcements form equilateral triangles. The behavior about the rigidity of an isogrid is isotropic within the plane of the structure, thus the term *'iso'* is given in reference to its isotropy. For some researchers, isogrid represents all lattice structures, even those that are not isotropic in any sense [36].

One of the first studies of rigid strut structures was conducted by NASA (National Aeronautics and Space Administration) in partnership with McDonnell Douglas Aeronautics Company (a company that was purchased by Boeing in 1996) which generated the first Handbook on isogrids structures. The study aimed to investigate new lightweight, economical and structurally efficient structures for aerospace application [37]. It cannot be said that the Isogrid Handbook developed by NASA was the first study in this area, since some Russian authors like [38] argue that the Soviet Space Program was the first to develop and apply isogrid in rockets and space vehicles such as Russian Proton-M.

In their work, [39] used unidirectional filament of carbon fiber and polymer matrix to fabricate structures of rigid ribs and to apply them in aircraft fuselages, rocket interstage and load adapters. For the accomplishment of the structural project, they used numerical simulation by the finite element method and analytical calculation (Eqs. 1, 2 Table 3). After the design of the structures, they performed the fabrication and then proceeded with the experimental tests to prove the design. With the results, they obtained 60% of reduction of mass of the fuselage structure and 40% of reduction for the interstage and adapters of load comparing with those made of aluminum.

Although some studies have been reported on isogrid composite structures, very few have been focused on the application on lower limbs amputees, i.e., for prosthesis design. The work presented here assesses the potential of a composite isogrid tube for a biomechanics application.

3 Experimental Methodology

This Section describes all stages of the development of the work from the beginning of the rigid tube design, going through the manufacturing process to the experimental trials.

3.1 Materials

The materials used in this work can be divided into two parts: material for the fabrication of test devices and materials for the process of fabrication of lattice structure tubes and structural inner layer. Following the manufacturing sequence of this work, the material used for the fabrication of the structural inner layer of rigid strand prosthetics tubes was ABS (Acrylonitrile Butadiene Styrene) polymer. The ABS of this work was brand ultimaker® and is commercially in the form of a filament for 3D printer. The filament has a diameter of 2.85 mm and can withstand temperatures up to 85 °C. For the manufacture of rigid composite material ribs, a continuous unidirectional carbon fiber filament was used from Hexcel Composites. The resin system used to manufacture the prosthetic tubes was Araldite® epoxy resin LY5052 and Aradur® 5052 hardener from the company Huntsman in the proportion of 100 g/38 g, respectively. Table 1 shows the materials properties for the materials in this study.

Table 1 Properties of T300 Unidirectional Carbon Fiber Composite/LY556/HT972 Epoxy Resin (adapted from [40])

Property	CFRP
Longitudinal Elasticity Modulus (E_1)	144 GPa
Transversal Elasticity Modulus (E_2)	6.5 GPa
In Plane Shear Module (G_{12})	5.6 GPa
In Plane Shear Resistance (S_{12})	40 MPa
Longitudinal Traction Resistance (X_{1T})	1200 MPa
Transversal Traction Resistance (X_{2T})	17 MPa
Longitudinal Compression Resistance (Y_{1C})	600 MPa
Transversal Compression Resistance (Y_{2C})	80 MPa
Interlaminar Shear (ILSS)	42 MPa
Density	1.35 g/cm^3
Poisson	0.21
Fiber volume	51%

3.2 Isogrid Tube Design and ABS Core

The initial phase of the lattice structure design and the structural inner layer can be divided into four steps: selection of lattice type configurations, structural analysis, design of structures and computational modeling for numerical simulation using the finite element method. The load condition values of the rigid ribs were selected as a function of the higher load level, i.e., for 2240 N (test), 4480 N (failure) compression and 7.1 Nm (failure) torsion. In this work, only static tests were performed because of the number of configurations to be studied, since the cyclic test must be performed in each test body with a frequency of 1 Hz until it reaches 3×10^6 cycles, i.e., the time spent would make this work unfeasible.

3.2.1 Isogrid Configurations Selection

The selection of the types of configurations of the rigid ribs and consequent application of these structures as tubes for prosthesis of lower limbs were based on the literature. As discussed in Section 2, some authors [39, 41] studied and optimized rigid strut structures as a function of the angle φ of the helical ribs. Due to these studies, the present work sought to select three types of configurations of lattice structures varying the angle φ. The three angles selected, and their respective justifications are set out in Table 2.

After defining the configurations of the structures to be studied in this work and in order to simplify the writing and for the better understanding of the reader, we adopted the terminology

Table 2 Selection of the types of lattice structures as a function of the angle φ

Isogrid structure	Angle φ	Reason
1	26°	A study by [39], stating that this is the optimal angle for lattice structures being requested by predominantly compression forces.
2	30°	A study conducted by [41] stating that this is the optimal angle for rigid strut structures being requested by predominantly compressive stresses.
3	40°	Adopted by the Author to analyze the influence of a larger angle on the properties of the requested structure by multi-loads.

CF26 ($\varphi = 26°$) for Structure 1, CF30 ($\varphi = 30°$) for Structure 2 and CF40 ($\varphi = 40°$) for Structure 3.

3.2.2 Analytical Calculations of Lattice Structures

In the initial design phase of open rigid strut structures (without the outer shell layer), the mathematical basis for the characterization, validation and optimization of the structure is given as a function of eight variables: *i)* The diameter D and the length L of the structure; *ii)* The thickness h of the helical and circular; *iii)* The angle φ of the helical ribs with respect to the axial axis of the structure; *iv)* The width δ_c and δ_h of the circular and helical ribs, respectively and *v)* The distance α_c and α_h of the circular and helical ribs, respectively, relative to the axial axis of the frame. Figure 4 illustrates the location of the eight design variables proposed by [39].

Because they have a predominantly axial load, the lattice structures are designed following Eq. 1.

$$P = F + \frac{4M}{D} \tag{1}$$

where F is the compression force of the design and M the moment in the structure.

Considering the second method, the optimal parameters for mass minimization are calculated by Eq. 2.

$$\overline{h} = \frac{h}{D}, \quad \varphi, \quad \overline{\delta}_c = \frac{\delta_c}{\alpha_c}, \quad \overline{\delta}_h = \frac{\delta_h}{\alpha_h} \tag{2}$$

In addition, there are three cases that depend on load normalization factors. The equations for the three cases are shown in Table 3.where $\overline{\sigma}$ is the rupture stress of the helical ribs, k is the buckling coefficient ($k = 1$) for structures with articulated joints and $k = 4$ for structures with fixed joints), E the modulus of elasticity in the main direction of loading, ρ is the density of the material used, $\overline{\rho} = \rho_c/\rho_h$, indices h and c refer to helical and circular respectively.

From the choice of the three angles, the analytical calculations were performed. For the analytical calculation of Structures 1, 2 and 3, the formulations used count on 20 project variables, being 10 dependent and 10 independent. Therefore, it was necessary to
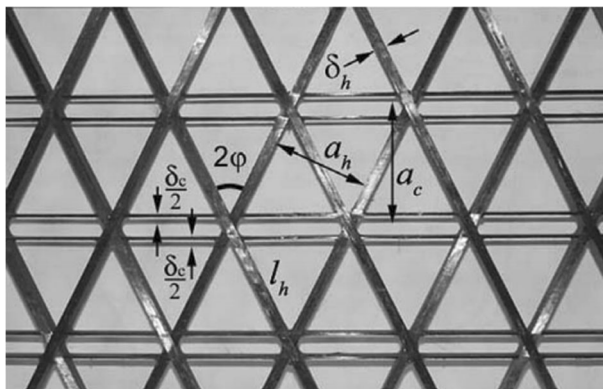
Fig. 4 Geometric parameters of rigid strut structure (adapted from [39])

Table 3 Structural Optimization Cases (adapted from [39])

Case 1	Case 2	Case 3
$p \leqslant p_s$	$p_s \leqslant p \leqslant p_o$	$p_o \leqslant p$
$\overline{h} = \dfrac{1}{4}\left(\dfrac{48\pi^4 k^2 \overline{\rho}^3}{E_h E_c^3}p^4\right)^{1/10}$	$\overline{h} = \dfrac{1}{4}\left(\dfrac{\pi^2 k\overline{\rho}}{E_c\overline{\sigma}}p^2\right)^{1/4}$	$\overline{h} = \dfrac{\pi p}{16\overline{\sigma}}\sqrt{\dfrac{kE_h p_s}{3\overline{\sigma}p_o}}$
$\mathrm{tg}\varphi = \dfrac{1}{2}$	$\mathrm{tg}^2\varphi = \dfrac{p_s}{4p}$	$\mathrm{tg}^2\varphi = \dfrac{p_s}{4p_o}$
$\overline{\delta}_h = \dfrac{5}{4\pi}\left(\dfrac{108\pi^2 E_c p^2}{E_h^3 k^4 \overline{\rho}}\right)^{1/10}$	$\overline{\delta}_h = \dfrac{2}{\pi\sin2\varphi}\sqrt{\dfrac{3\overline{\sigma}}{kE_h}}$	$\overline{\delta}_h = \dfrac{2}{\pi\sin2\varphi}\sqrt{\dfrac{3\overline{\sigma}}{kE_h}}$
$\overline{\delta}_c = \dfrac{\overline{\delta}_h}{2\overline{\rho}}$	$\overline{\delta}_c = \dfrac{p_s\overline{\delta}_h}{2\overline{\rho}p}$	$\overline{\delta}_c = \dfrac{p_s p_o \overline{\delta}_h}{\overline{\rho}p^2}\left(\dfrac{p_o^2}{p^2}-\dfrac{1}{2}\right)$

determine the values for the independent variables to find the dependent variables. Thus, the values adopted for the independent variables as well as their justifications are set out in Table 4.

Obtaining the values of the dependent variables through the analytical calculations was of paramount importance for this work, since some variables such as the thickness of the rigid ribs and the distance between the helical and circular rigid ribs could be identified.

### 3.2.3 Design of Rigid Ribs and Inner Layer Structures

In the design stage in CAD, the lines of revolution of the helical rigid ribs were generated according to their angle φ. For example, for Structure 1 with angle φ of 26 ° and with the

Table 4 Definition of the values of the project-independent variables

#	Variable	Value	Reason
1	Diameter (D)	30 mm	The diameter value was chosen according to the diameters of the prosthetic tubes present commercially and in the literature.
2	Length (L)	300 mm	The length value was chosen based on the lengths of the prosthetic tubes present commercially and in the literature.
3	Angle φ	26°, 30° e 40°	See Table 2
4	Width of helical ribs (δ_h)	4 mm	The width adopted corresponds to the width of the continuous filament of carbon. Due to the small diameter of the structure, the increase of the width of the ribs would imply an increase of the surface and consequent increase of mass, against the objectives of this work
5	Width of circular ribs (δ_c)	4 mm	In the case of the same material used for helical rigid ribs (reason 4)
6	Modulus of Elasticity of Helical ribs (E_h)	144 GPa	The Elasticity modulus adopted corresponds to the carbon fiber/epoxy resin composite module.
7	Circular ribs elasticity module (E_c)	144 GPa	In the case of the same material used for the helical rigid ribs
8	Rupture Stress (σ)	1200 MPa	The rupture stress adopted corresponds to the composite carbon fiber/epoxy composite module.
9	Specific gravity of helical ribs (ρ_h)	1.35 g/cm^3	The specific mass adopted corresponds to the specific mass of the carbon fiber/epoxy resin composite.
10	Specific mass of circular ribs (ρ_c)	1.35 g/cm^3	In the case of the same material used for helical rigid ribs (reason 9)

knowledge of the values of the diameter and the length of the structure one can obtain the value of the lines of revolution of each rigid plate by basic trigonometry. Thus, the design of CF26, CF30 and CF40 can be realized and generated the surfaces (shells) of their respective helical and circular ribs (Fig. 5a, b, c). From the design of the surfaces of the rigid helical and circular ribs of each structure, it was possible to design the internal structural layer that is also part of the objectives of this work. The inner layer has cavities to "accommodate" the helical and circular rigid ribs (Fig. 5d).

In this work, the modeling of all structures, including the inner coating layer and the helical and circular rigid crosspieces, were made through 2D shell elements. This type of modeling is widely used in the area of projects involving numerical simulation, since it guarantees good results at the same time, it entails a low computational cost [15, 42]. The elements used were the QUAD and TRIA of the OptiStruct® element library. The QUAD element has four nodes and six degrees of freedom per node and the TRIA element with three nodes and also six degrees of freedom per node. After several tests with different mesh size, based on the best cost/convergence, the average element size was defined as 1 mm.

(a)

(b)

(c)

(d)
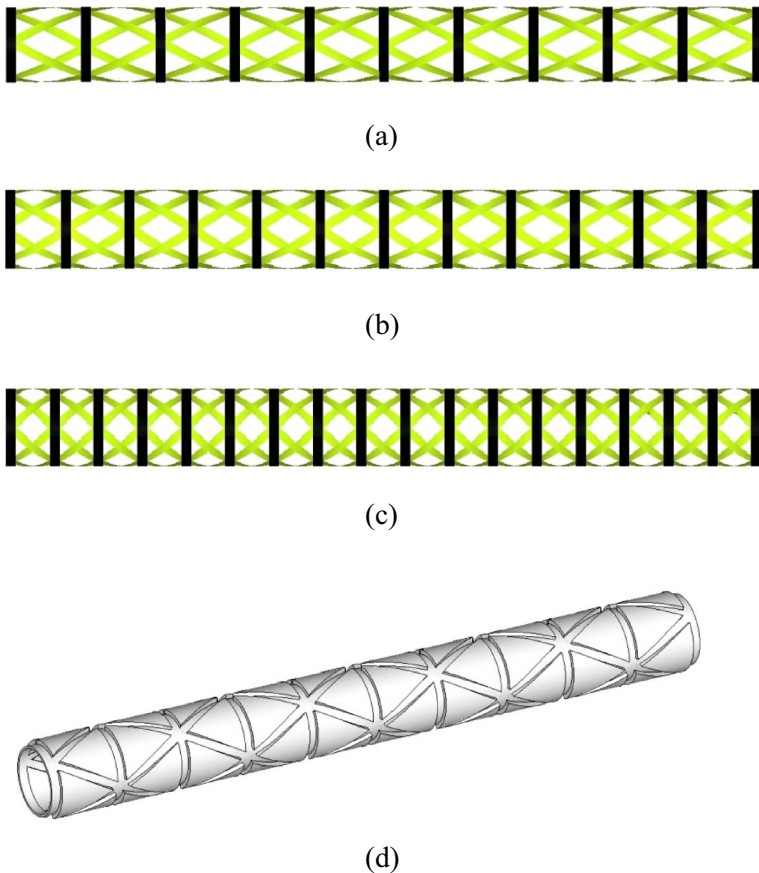
Fig. 5 Isogrid strucutres (**a**) CF26, **b** CF30, **c** CF40 and the inner layer of structure CF26 (**d**)

After the creation of the mesh, the orientation of the composite was defined following a manufacturing process, that is, the orientations of the rigid helical and circular ribs were in the same direction as the winding of the carbon fibers. This step has great importance to guarantee good results, because if it is a composite material that has anisotropic mechanical behavior, the correct orientation of the laminate directly implies the response of the structure when requested by external loading.

After defining the boundary conditions, the Tsai-Wu fault criterion [43] was selected for the static linear analysis of the structures. The failure criterion proposed by [43] establishes equations for a stress analysis for anisotropic materials. Briefly, a laminate would fail according to Eq. 3.

$$F = F_1\sigma_1 + F_{11}\sigma_1^2 + F_2\sigma_2 + F_{22}\sigma_2^2 + 2F_{12}\sigma_1\sigma_2 + F_{66}\tau_{12}^2 < 1.0 \qquad (3)$$

where:

$$F_1 = \frac{1}{X_{1T}} - \frac{1}{Y_{1C}} \qquad (4)$$

$$F_{11} = \frac{1}{X_{1T}Y_{1C}} \qquad (5)$$

$$F_2 = \frac{1}{X_{2T}} - \frac{1}{Y_{2C}} \qquad (6)$$

$$F_{22} = \frac{1}{X_{2T}Y_{2C}} \qquad (7)$$

$$F_{66} = \frac{1}{S_{12}^2} \qquad (8)$$

$$F_{12} = \frac{1}{2P^2}\left[1 - P\left(\frac{1}{X_{1T}} - \frac{1}{Y_{1C}} + \frac{1}{X_{2T}} - \frac{1}{Y_{2C}}\right) - P^2\left(\frac{1}{X_{1T}Y_{1C}} + \frac{1}{X_{2T}Y_{2C}}\right)\right] \qquad (9)$$

where σ_1, σ_2 and τ_{12} are the principal stresses and $P = \sigma_1 = \sigma_2$ assuming biaxial stresses [43]

As previously described, numerical simulations were performed for each structure proposed by this work and for each type of loading according to the standard. In order to calculate the safety margins (MoS) of the structures according to the Failure Index of the Tsai-Wu criterion, we have Eqs. 10 and 11.

$$MoS = SR - 1 \qquad (10)$$

$$SR = \frac{1}{FI} \qquad (11)$$

where SR is the resistance factor and is inversely proportional to the maximum failure index (FI) of the Tsai-Wu criterion.

After the design of the CF26, CF30 and CF40 structures, the manufacturing process began, which can be divided into three steps: inner layer fabrication, carbon fiber positioning in the inner layer and processing of structures via VARTM.

3.3 Internal Core Manufacturing

For the fabrication of the inner layer of structural support, this work made use of 3D printing which is an additive manufacturing process. Basically, the process consists in melting the material and then depositing it in layers to form the desired structure. The 3D printer used in this work was an Ultimaker 2® with a print volume of 120x120x115mm.

After adjusting the 3D printing parameters, it was possible to fabricate the inner layers of the CF26, CF30 and CF40 structures. As discussed earlier, the maximum print height of the Ultimaker 2® is 115 mm, so it was necessary to divide the 300 mm tube into four 75 mm pieces and then attach them in a single tube. To ensure the precision of the joints, internal flanges have been designed for positioning the parts. Figure 6 illustrates the 3D impression of a part of the inner layer of the CF26 structure and its complete assembly.

Thus, all inner layers of the CF26, CF30 and CF40 structures have been printed and assembled for the next manufacturing step. The 3D impression of the inner layer was of great importance for this work, as well as serving as a structural part of the prosthetic tube, served to ensure the accuracy of the winding of the layers of carbon fiber in the correct positions and angles.

3.4 VARTM Processing

From the coiling of the dried fibers in all specimens of the CF26, CF30 and CF40 structures, the resin infusion process was started via VARTM. Briefly, in this process the fiber layers (laminate) are positioned against a mold and wrapped in a plastic film whose purpose is to compact the laminate and at the same time serve as a flexible counter mold [44]. Then the addition of consumable materials (release fabric, transport media, resin transport duct) and closure of the system using an edge sealant tape is performed. For the application of the

Fig. 6 Printing the inner layer of the CF26
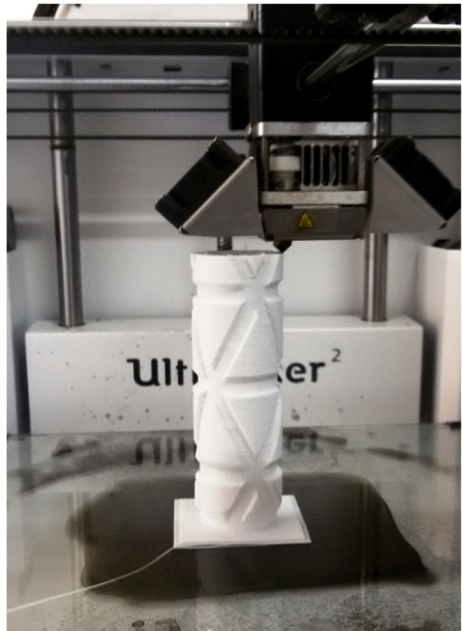
vacuum, a vacuum pump connected to an outlet for the resin is used. Thus, with the aid of the vacuum, the resin is infused through the laminate causing impregnation of the fibers.

To begin the resin infusion process via VARTM of the rigid header tubes, the first step was to cut the vacuum bag and place it on a work table. The application of the edge sealant was performed around the region where the structure would be positioned. Then, two pieces of release fabric (peel ply) were cut to coat the structure and facilitate its demolding. The peel-coated ply structure was positioned over the vacuum bag and the resin transport medium was inserted.

Then, two infusion line registers were positioned at the ends of the vacuum bag and over the edge sealant. Two spiral hoses (Spiraduto) were placed in each register to ensure a better distribution of the resin. These registers along with the Spiradutos are responsible for the resin inlet and vacuum outlet. The next step was to close the vacuum bag (Fig. 7), whereupon the protection (White) of the edge sealant was removed and the vacuum bag was carefully positioned throughout the region of the edge sealant. Two hoses were connected at the end of infusion line records, one at the resin inlet and one at the vacuum outlet. At the resin inlet, a funnel was inserted to facilitate the infusion process and at the outlet of the vacuum the hose was connected to the vacuum pump.

The vacuum pump is then driven with a pressure of approximately 25 mPa to ensure that there are no regions with air leaks preventing bubbles from occurring at the time of infusion of resin. Vacuum application ensures compactness of the fiber layers as well as assist in uniform fiber impregnation.

After the application of the vacuum and the inspection to ensure that there were no leaks, the resin infusion procedure was started. With the aid of a mixer, parts A and B of the resin system were mixed for a period of 4 min. Thus, the mixture was poured into the funnel and the record of the resin infusion line was opened. With the aid of vacuum, the carbon fibers were fully impregnated by the resin. After the process was completed, the vacuum bag with the structure was taken to a greenhouse with a heating ramp of 5 °C/min until reaching 80 °C of landing temperature and remaining for 4 h at 80 °C to ensure complete healing. All this procedure described above was applied to all test specimens of all structures proposed by this work.

### 3.5 Compression Test of the Partial Structure (Transtibial)

According to the standard, the compression tests were divided into two stages: Evidence and Failure. For the test of proof a total of nine tubes were used, being three of each structure (CF26, CF30 and CF40) all with length of 300 mm. As discussed earlier, if the test bodies did not fail the test of proof, they could be used in the compression test until failure. For both tests (Proof and Failure), the supports (Fig. 8) were designed to ensure a better distribution of the compression load and to prevent the tubes from slipping in the tests.

The test specimens were placed in the universal test machine and thus, the test was started with a velocity of 2 mm/min. Upon reaching 2240 N the test was interrupted, as described in

Fig. 7 Vacuum bag closing

<div align="center">(a)   (b)</div>
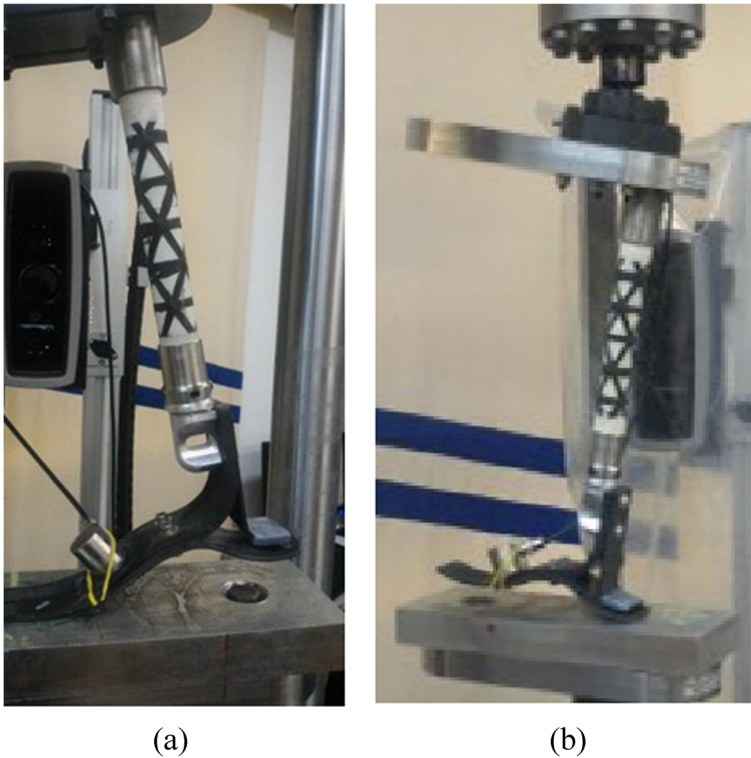
Fig. 8 Front test position (**a**) and heel (**b**)

standard NBR ISO 10328: 2002. All test specimens that were approved, that is, did not break before the test load, and were retested until failure.

For the calculation of the compressive strength and modulus of elasticity of the rigid tube tubes, Eqs. 12 and 13 respectively were used.

$$\sigma = \frac{F}{A_{tr}} \tag{12}$$

$$E = -\frac{\Delta\sigma}{\Delta\varepsilon} \tag{13}$$

where σ is the compressive strength (MPa), F is the force applied in (N), A_{tr} is the cross-sectional area of the lattice tube, E is the modulus of elasticity in (GPa), $\Delta\sigma$ is the variation between the initial and final compression strength, $\Delta\varepsilon$ variation between the initial and final deformation.

According to NBR ISO 10328: 2002, a partial (transtibial) structure involves the prosthetic tube, the prosthetic tube support and the foot/heel joint (Fig. 2). By default, the transtibial structure must pass the test of evidence and failure and both the front (prosthetic foot) and the back (prosthetic heel) in both modalities must be tested. In order to carry out the foot/heel test, the transtibial structure was assembled according to the standard that establishes the slopes and

angles for force application. Figure 8a and b illustrate the positioning of the transtibial structure for the front and rear test configurations, respectively.

After the positioning of the structure in the universal servo-hydraulic test machine of the brand Instron, model 8801, the test speed was 2 mm/min. The loading criteria to be applied in the transtibial structure are shown in Table 5. In addition, Fig. 9 illustrates the flowchart with the stages of the development of this work.

4 Numerical-Experimental Results and Discussion

In this section, the numerical simulation results will be analyzed and discussed by the finite element method for lattice structures with and without the inner layer. As previously pointed out, the purpose of analyzing only the rigid strut structure was to verify the influence of the inner layer on the mechanical properties of the prosthetic tube as the increase of the resistance to compression or torsion.

4.1 Numerical Results

In this step, the numerical simulation was performed to evaluate if the structures CF26, CF30 and CF40 would support the load of 7.1 N·m without the presence of the inner layer. The results are shown Fig. 10. The criterion used to evaluate whether the structures are failing was that of Tsai-Wu. It can be seen from Fig. 10 the example of the numerical results for torsion. For a better interpretation of the results, the safety margin calculation was calculated and the results are presented in Table 6.

As can be seen from Table 6, the safety margins are very high, with the smallest margin being the CF26 structure. The CF30 and CF40 structures have the highest safety margins and both are the same. In addition, the CF26 structure is less efficient in torsion compared to the CF30 and CF40 structures, however, all structures meet the standard with a large margin of safety. Thus, in descending order of resistance to torseness the structures CF40, CF30 and CF26 appear. The numerical torsional simulation results for the CF26, CF30 and CF40 lattice structures with the inner layer are shown in Fig. 10. The same parameters adopted previously were used in this simulation, with the difference that it has the inner layer of ABS. For a better interpretation of the results, the safety margin calculation (*MoS*) was also calculated from Eqs. 8 and 9 and the results are presented in Table 6.

Analyzing Table 6 it can be seen that the safety margins increased greatly with the inclusion of the inner layer in the structure. In addition, there was a reversal of the *MoS* values with the use of the inner layer. In descending order of torsion resistance CF26, CF30 and CF40 structures appear. This means that the inner layer increases the torsional strength of the structures.

Table 5 Static tests transtibial structure

Load condition	Proof test	Failure test
I(applied to the Heel)	2240 N	4480 N
II (applied in Foot)	2013 N	4025 N
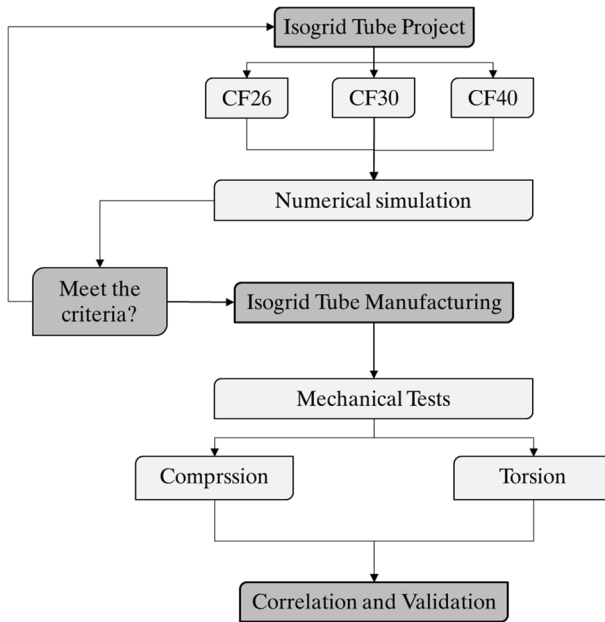
Fig. 9 Flowchart of the stages of work development

Using the same methodology for compression simulations, the structures were first analyzed without the inner coating layer. The proofing step was discarded at this stage of numerical simulation because the structures must be robust enough to withstand the loading of 4480 N, so the 2240 N load of the verification test becomes irrelevant because it has a lower
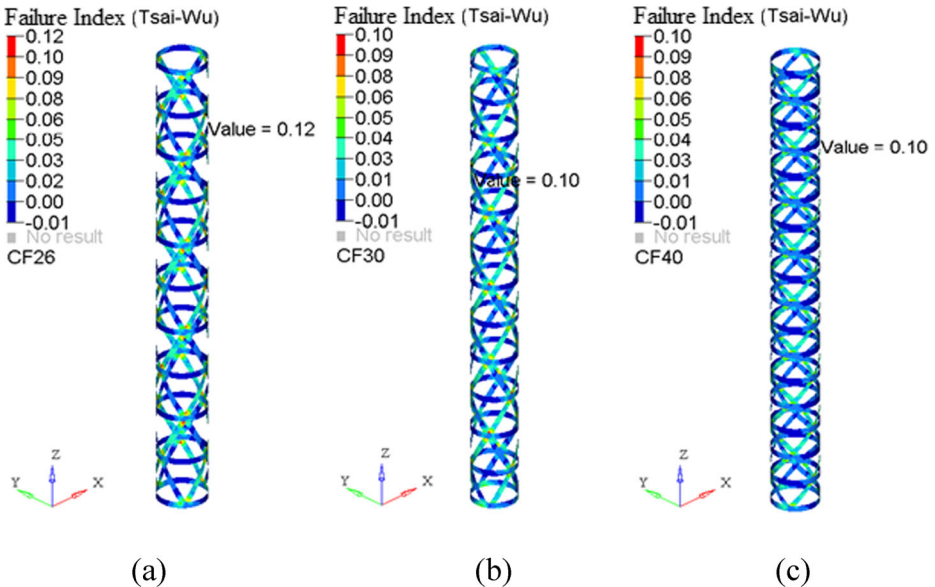
Fig. 10 Isogrid Tsai-Wu failure criteria results for torsion for the tube (**a**) CF26 (**b**) CF30 and (**c**) CF40

Table 6 The torsion values of the safety margin for rigid ribs with and without inner bed

Structure	Torsion		Torsion (with ABS core)		Compression		Compression (with ABS core)	
	FI	MoS	FI	MoS	FI	MoS	FI	MoS
CF26	0.12	7.3	0.045	21.2	0.87	0.15	0.79	0.27
CF30	0.10	9.0	0.049	19.4	0.87	0.15	0.73	0.37
CF40	0.10	9.0	0.063	14.9	1.11	−0.10	0.68	0.47

value. Thus, Fig. 10c and d illustrates the compression results for CF26, CF30 and CF40 structures without the presence of an inner layer. It can be seen that the CF26 and CF30 structures are meeting the standard compression failure requirements but with tight safety margins. Regarding the CF40 structure, it is failing before reaching the 4480 N compression load stipulated by the standard. In descending order of compressive strength are CF26, CF30 and CF40 structures. By the results of, the structures with inner layer had increased the compressive strength. Therefore, all were approved in the requirements of the standard, even the CF40 structure that was previously being disapproved. In addition, following the same tendency of the torsion results, with the inclusion of the inner coating layer, there was an inversion of the compressive strength values and in descending order are the structures CF40, CF30 and CF26.

With the objective of evaluating the maximum values of compressive strength to failure, as for the torsion resistance, several numerical simulations (interactive methods) were carried out to reach the maximum compressive load value that the different types of pipe configurations would withstand. Figure 10c illustrates the numerical modeling with the maximum compressive load obtained for each type of structure. Figure 10d shows the failure analysis of the rigid struts structures and the inner layer of ABS.

The maximum values, in compression, found for all CF26, CF30 and CF40 structures were 5100 N, 6000 N and 7000 N respectively, all above the requirement of the standard. The inner layers of ABS for all structures are not flawed, since the flow limit is 39 MPa.The works of [39] and of [41] state that lattice structures with angles of 26° and 30°, respectively, have the best mechanical properties in compression. These results, if confirmed experimentally, especially those of inversion of values when inserted the inner layer in the structures, show that a more improved mathematical model is necessary to predict the behavior of structures of rigid ribs with inner layers.

This inversion of values occurs due to some factors: The structure of lattices, without the use of the inner layer of polymer, is formed by the carbon fiber composite and epoxy resin where the characteristics related to the mechanical properties are influenced only by the orientation of the fibers (reinforcement). When the inner layer is part of the structure, the composite is formed by carbon fiber, epoxy resin and ABS polymer. Thus, there is the modification of the mechanical properties of the structure which depend not only on the orientations of the fibers, but also on the amount of reinforcement. In addition, an analysis of Fig. 10c and d showed that the higher tensions in the inner layers occurred in the structures that supported the larger loads. This shows that a portion of the load which was previously supported only by the rigid ribs has been transferred to the ABS polymer which in turn contributes to the increase in rigidity of the structure.
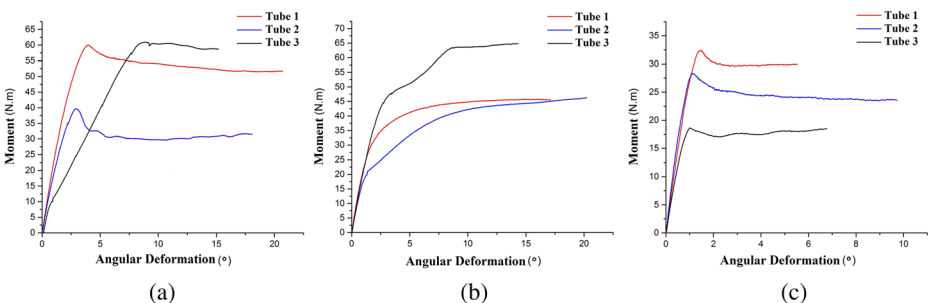
4.2 Experimental Results

After analyzing the results of numerical simulations for both torsion and compression, an experimental analysis of the results through mechanical tests was of paramount importance for the criterion of proving the structure. In addition, from the mechanical tests required by the standard it was possible to calculate the correlation of numerical and experimental results. Thus, in this chapter the results of the mechanical torsion and compression tests of the CF26, CF30 and CF40 structures will be presented, as well as the result of the test of the partial structure in compression. For the torsion tests, three lattice tubes were manufactured for each structure. The results for structure CF26, CF30 and CF40 are shown in Fig. 11a, b and c, respectively.

At first, analyzing the curves of Fig. 11a, b and c, it is assumed that the tubes failed because they have "peaks" where the structures reach higher values and then fall and remain constant. The fact was that in the tests, this peak and the constant values represent the beginning and the continuity of the sliding of the tubes. Due to problems of fixing the specimens to the test device, after a certain time, the device rotated without transferring the charge to the tubes. Thus, in this test it was not possible to fail the specimens in order to obtain the maximum torsional loading of each type of configuration. However, all specimens of all configurations obtained higher values of torsion resistance than required by the standard and some specimens, such as CF26 Tube 1 and CF30 Tube 3, obtained values above 60 N.m.

Figure 12a, b and c show the behavior of the specimens of structures CF26, CF30 and CF40, respectively. The differences with respect to the curves at all curves were due to the accommodation of the tubes in the test device. According to the norm, an initial load of 100 N should be applied for the accommodation of the tubes, but this loading was not sufficient for some specimens, generating this difference between the curves. However, all prosthetic tubes of the CF26, CF30 and CF40 structures reached the value of 2240 N required by [45]. Thus, these tubes could be tested until failure.

As discussed previously in this work, in order to measure the impact absorption energy of the rigid header tubes, the Charpy impact test was performed. Table 7 shows the impact energy absorption results for the CF26, CF30 and CF40 structures for the inner layer and for the Carbon Fiber/Epoxy Resin Tube.

From the results of Table 7 it was possible to observe that the CF26 and CF30 structures have energy absorption values very close to the CFRP Tube, and the CF40 structure has a further 12 J. Thus, the rigid header tubes proposed by this work have an excellent impact resistance. Figure 13 illustrates all structures tested on impact.

Fig. 11 Mechanical tests results for torsion (**a**) CF26, (**b**) CF30 and (**c**) CF40
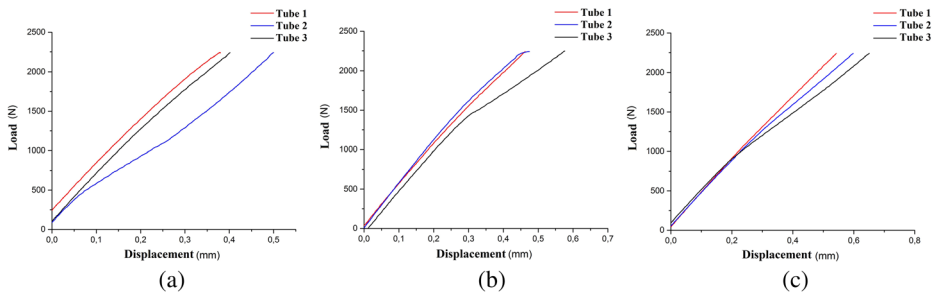
Fig. 12 Mechanical tests results in compression for (**a**) CF26, (**b**) CF30 and (**c**) CF40

4.3 Analysis of the Partial Structure

In Section 3 the experimental method for compression testing of the partial structure with loading applied to the prosthetic foot and the prosthetic heel was discussed. At first, the partial structure test for both cases was performed only with the structure tube CF26. This was due to the high time of manufacture of the specimens, so only the CF26 structure was finalized in time for the assay. However, it is expected that the CF30 and CF40 structures show a tendency for better results than the CF26 structure.

The results of the compression test of the partial structure with point of loading of the foot and the prosthetic heel are shown by the curves of Fig. 14a. By means of the curves of Fig. 14b it can be seen that the partial structure with the tube CF26 was successful in the verification test. The results of the rupture test for the partial structure with point of loading of the foot and the prosthetic heel are illustrated by the Fig. 15.

By analyzing the results of the Fig. 14 it was possible to evaluate that the partial structure with the CF26 tube was approved in the requirements of the standard in view that it reached the load of rupture 4445 N for the foot and 4794 N for the heel being required by the standard 4025 N and 4480 N, respectively.

It is worth mentioning that the static loads proposed by NBR ISO 10328: 2002 are far beyond the maximum values found in the tibia and fibula bones of a person walking or running. In his work, [46, 47] studied the forces applied to the tibia and fibula bones of a person moving or walking using sensors in 20 male and female patients of various ages for 5 uninterrupted months. Thus, it was concluded that the value of the maximum force peak was 728.6 N. Therefore, achieving the values of the standard guarantees the safety of the project. Figure 15 illustrates tube failures in the foot and heel compression tests, respectively.

Table 7 Impact energy absorption result

|	CF26	CF30	CF40	Internal core	Tube CFRP
Tube1	58 J	50 J	62 J	1 J	56 J
Tube 2	57 J	62 J	78 J	1 J	54 J
Tube 3	54 J	60 J	76 J	1 J	70 J
Average	56 J	57 J	72 J	1 J	60 J
Std. Deviation	2 J	6 J	9 J	0 J	9 J
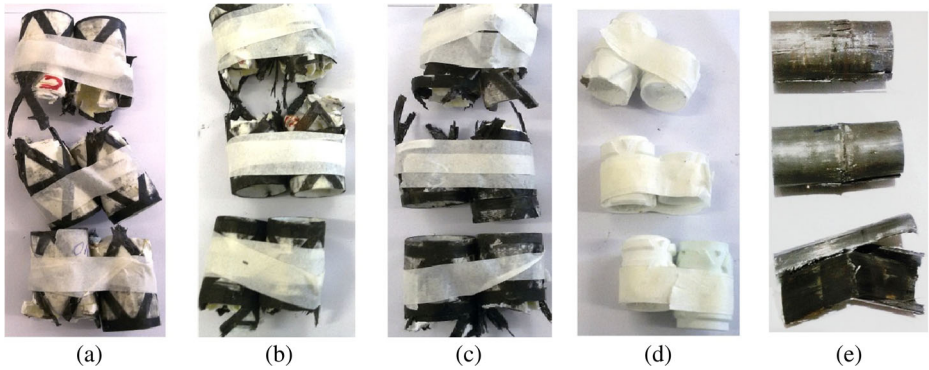
Fig. 13 Result of failures in the impact test (**a**) CF26, (**b**) CF30, (**c**) CF40, (**d**) Inner layer and (**e**) CFRP tube

5 Conclusion

In the present work, the feasibility of a new tube concept, made of composite material, was evaluated using a rigid strut structure and structural inner layer for application as a transtibial prosthesis tube. From the structural point of view, the use of an inner layer in rigid tube tubes proved very efficient and very promising. The inner layer can be considered as part of structural support because it directly implies numerical and experimental results for lattice structures, since their inclusion in the structure modifies the optimal parameters already proposed in the literature.

The results showed that all lattice structures proposed by this work have the feasibility to be used as a tube for transtibial prostheses. The CF40 structure presented the best results and is best suited to be used as a prosthetic tube. CF26 and CF30 can also be used as a prosthetic tube because they have met the requirements of the standard but are less efficient.

The manufacture of rigid inner tube tubes is not feasible from the industrial point of view, since the manual winding of the fiber, the fabrication of the layer through 3D printing and the infusion of resin by VARTM lead to a slow manufacturing process. This manufacturing process was used to test the concept of the structure that uses the structures of rigid ribs and inner layer. The results showed that the concept was successfully approved and could be used as a prosthetic tube. Thus, one way to streamline manufacturing and increase productivity
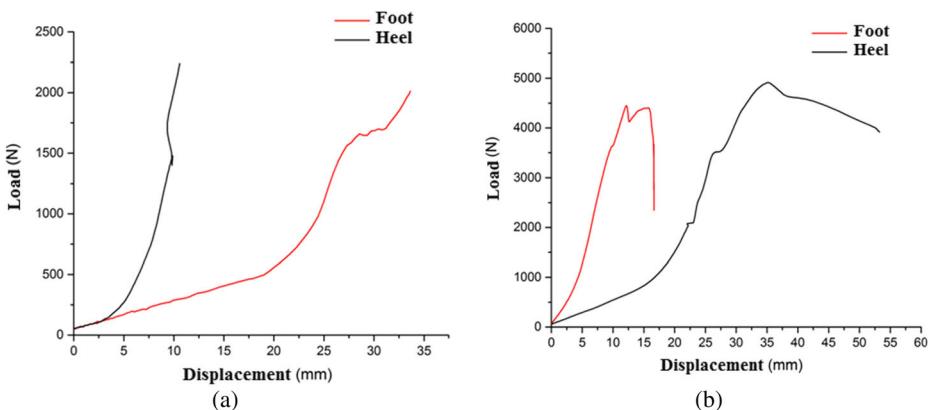
Fig. 14 Static test of proof (**a**) and rupture (**b**) for the partial structure

(a)   (b)
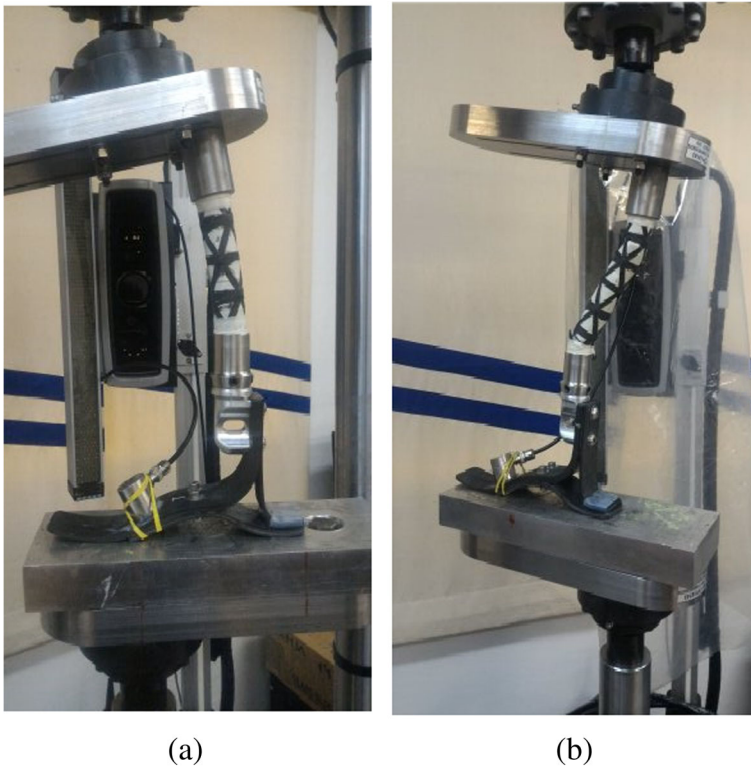
Fig. 15 Failure of the tubes in the foot (**a**) and heel (**b**)

would be to implement the winding of the fibers in a filament winding machine and to make a polymer injection tool for scaling the inner layers. Thus, the process would have agility and could go into scale of industrial production.

Compliance with Ethical Standards

Conflicts of Interest The authors declare that they have no conflict of interest.

References

1. Gard, S.A., Konz, R.J.: The effect of a shock-absorbing pylon on the gait of persons with unilateral transtibial amputation. J. Rehabil. Res. Dev. **40**(2), 109–124 (2003)
2. Shasmin, N., et al.: A new pylon materials in transtibial prosthesis: a preliminary study. J. Biomech. **40**, S297 (2007)
3. Bliquez, L.V.: Classical prosthetics. Archaeol. Inst. Am. **36**(5), 25–29 (1983)
4. Norton, K.: A brief history of prosthetics. InMotion. **17**(7), 1–3 (2007)
5. Benhamou, R.: The artificial limb in preindustrial France. Technol. Cult. **35**(4), 835–845 (1994)

6. Nolan, L.: Carbon fibre prostheses and running in amputees: a review. Foot Ankle Surg. **14**(3), 125–129 (2008)
7. Phillips, V. L. Composite Prosthetic Foot and Leg USA (1983)
8. Vilagra, J., Sganzerla, C., Walcker, L.: Próteses transtibiais: itens de conforto e segurança. Rev. Thema Sci. **1**(2), 107–112 (2011)
9. Scholz, M.S., Blanchfield, J.P., Bloom, L.D., Coburn, B.H., Elkington, M., Fuller, J.D., Gilbert, M.E., Muflahi, S.A., Pernice, M.F., Rae, S.I., Trevarthen, J.A., White, S.C., Weaver, P.M., Bond, I.P.: The use of composite materials in modern orthopaedic medicine and prosthetic devices: a review. Compos. Sci. Technol. **71**(16), 1791–1803 (2011)
10. Shasmin, H.N., Abu Osman, N.A., Abd Latif, L.: Economical tube adapter material in below knee prosthesis. IFMBE Proc. **21**(1), 407–409 (2008)
11. Giest, T.N., Chang, Y.H.: Biomechanics of the human walk-to-run gait transition in persons with unilateral transtibial amputation. J. Biomech. **49**(9), 1757–1764 (2016)
12. Silverman, A.K., Neptune, R.R.: Muscle and prosthesis contributions to amputee walking mechanics: a modeling study. J. Biomech. **45**(13), 2271–2278 (2012)
13. Winter, D.A., Sienko, S.E.: Biomechanics of below-knee amputee gait. J. Biomech. **21**(5), 361–367 (1988)
14. Major, M.J., Twiste, M., Kenney, L.P., Howard, D.: Amputee independent prosthesis properties—a new model for description and measurement. J. Biomech. **44**(14), 2572–2575 (2011)
15. Carroll, K., Sabolich, S.: Below-Knee Prosthetics. Is It Time For An Upgrade? INMotion Mag. **9**(4), 1 (1999)
16. Junqueira, D.M., Silveira, M.E., Ancelotti Junior, A.C.: Analysis of spot-weld distribution in a weldment — numerical simulation and topology optimization. Int. J. Adv. Manuf. Technol. **1**, 1–9 (2018)
17. Lee, W.C.C., Zhang, M.: Fatigue test of low-cost flexible-shank monolimb transtibial prosthesis. Prosthetics Orthot. Int. **30**(3), 305–315 (2006)
18. Rothschild, V., et al.: Clinical experience with total thermoplastic lower limb prostheses. J. Prosthet. Orthot. **3**(1), 51–54 (1990)
19. Valenti, T.: Experience with Endoflex: A Monolithic Thermoplastic for Below-Knee Amputees. J. Prosthet. Orthot. **3**(1), 43–50 (1990)
20. Ancelotti, A. C. Efeitos da porosidade na resistência ao cisalhamento e nas propriedades dinâmicas de compósitos de fibra de carbono/resina epóxi – Doctoral Thesis-Technological Institute of Aeronautics (2006)
21. Lebrão, G. W.: Viabilidade De Fabricação De Tubo Para Prótese De Membro Inferior Em Compósito Híbrido Epóxi Carbono-Vidro. [s.l.], Doctoral Thesis - Universidade de São Paulo (2007). https://doi.org/10.11606/D.85.2007.tde-25062007-163320
22. Martins, A. T. D.: Projeto e Fabricação de Tubos Compósitos em Fibras de Carbono/Epóxi para Próteses Transtibiais por Moldagem com Bladder. Master in Engineering Thesis - Universidade Federal de Itajubá (2015)
23. Wilson, M. T.: Composite pylon for a prosthetic device. U.S. Patent Application n. 14/483,281, 12 mar. 2015
24. Fey, N.P., Klute, G.K., Neptune, R.R.: The influence of energy storage and return foot stiffness on walking mechanics and muscle activity in below-knee amputees. Clin. Biomech. **26**(10), 1025–1032 (2011)
25. Sam, M., Childress, D., Hansen, A., Meier, M., Lambla, S., Grahn, E., Rolock, J.: The "Shape & Roll" prosthetic foot: I. Design and development of appropriate Technology for low-Income Countries. Med. Conflict Surviv. **20**(4), 294–306 (2004)
26. Kobayashi, T., Orendurff, M.S., Zhang, M., Boone, D.A.: Effect of alignment changes on sagittal and coronal socket reaction moment interactions in transtibial prostheses. J. Biomech. **46**(7), 1343–1350 (2013)
27. Kobayashi, T., Orendurff, M.S., Arabian, A.K., Rosenbaum-Chou, T.G., Boone, D.A.: Effect of prosthetic alignment changes on socket reaction moment impulse during walking in transtibial amputees. J. Biomech. **47**(6), 1315–1323 (2014)
28. Schwarze, M., Hurschler, C., Seehaus, F., Oehler, S., Welke, B.: Loads on the prosthesis-socket interface of above-knee amputees during normal gait: validation of a multi-body simulation. J. Biomech. **46**(6), 1201–1206 (2013)
29. Coleman, K.L., Boone, D.A., Smith, D.G., Czerniecki, J.M.: Effect of transtibial prosthesis pylon flexibility on ground reaction forces during gait. Prosthetics Orthot. Int. **25**(3), 195–201 (2001)
30. Gomes, G.F., Diniz, C.A., da Cunha, S.S., Ancelotti, A.C.: Design optimization of composite prosthetic tubes using GA-ANN algorithm considering Tsai-Wu failure criteria. J. Fail. Anal. Prev. **17**(4), 740–749 (2017)
31. Berge, J.S., Klute, G.K., Czerniecki, J.M.: Mechanical properties of shock-absorbing pylons used in transtibial prostheses. J. Biomech. Eng. **126**(1), 120–122 (2004)

32. Zheng, Q., Jiang, D., Huang, C., Shang, X., Ju, S.: Analysis of failure loads and optimal design of composite lattice cylinder under axial compression. Compos. Struct. **131**, 885–894 (2015)
33. Totaro, G.: Local buckling modelling of isogrid and anisogrid lattice cylindrical shells with triangular cells. Compos. Struct. **94**, 446–452 (2012)
34. Fan, H., Fang, D., Chen, L., Dai, Z., Yang, W.: Manufacturing and testing of a CFRC sandwich cylinder with Kagome cores. Compos. Sci. Technol. **69**(15–16), 2695–2700 (2009)
35. Totaro, G., De Nicola, F., Caramuta, P.: Local buckling modelling of anisogrid lattice structures with hexagonal cells: an experimental verification. Compos. Struct. **106**, 734–741 (2013)
36. Huybrechts, S. M.; Hahn, S. E.; Meink, T. E. Grid stiffened structures: a Survay of fabrication, analysis and design methods. 12 ICCM Proceedings, (1999)
37. Huybrechts, S.M., Meink, T.E., Wegner, P.M., Ganley, J.M.: Manufacturing theory for advanced grid stiffened structures. Compos Part A. **33**(2), 155–161 (2002)
38. Meyer, R. R.: McDonnell Douglas Astronautics Company, Isogrid Design Handbook. NASA Contractor Report, CIR-124075, Revision A (1973)
39. Vasiliev, V. V.; Razin, A. F. Optimal design of filament-wound anisogrid composite lattice structures. Proceedings of the 16th annual technical conference of American society for composites. Blacksburg USA, (2001)
40. Vasiliev, V.V., Razin, A.F.: Anisogrid composite lattice structures for spacecraft and aircraft applications. Compos. Struct. **76**(1–2), 182–189 (2006)
41. Madhavi, M., Rao, K.V.J., Rao, K.N.: Design and analysis of filament wound composite pressure vessel with integrated-end domes. Def. Sci. J. **59**(1), 73–81 (2009)
42. Sorrentino, L., Marchetti, M., Bellini, C., Delfini, A., Albano, M.: Design and manufacturing of an isogrid structure in composite material: numerical and experimental results. Compos. Struct. **143**, 189–201 (2016)
43. Silveira, M.E., Fancello, E.A.: O uso de otimização numérica no projeto de blanks soldados. Cienc. Eng/Sci. Eng. J. **24**(1), 9–19 (2015)
44. Tsai, S.W., Wu, E.M.: A general theory of strength for anisotropic materials. J. Compos. Mater. **5**(1), 58–80 (1971)
45. Handbook, Military. "MIL-HDBK-17-2F: composite materials handbook." Polym. Matrix. Compos. Mater. Usage. Des. Anal. 17 (2002)
46. NBR ISO 10328-1: Próteses - Ensaio Estrutural para Próteses de Membro Inferior: configurações de ensaio. Associação Brasileira de Normas Técnicas, Rio de Janeiro (2002)
47. D'Angeli, V., Belvedere, C., Ortolani, M., Giannini, S., Leardini, A.: Load along the femur shaft during activities of daily living. J. Biomech. **46**(12), 2002–2010 (2013)